New Carbon Materials 2021, 36(3): 573-584

Supporting Information

Reduced graphene oxide encapsulated MnO microspheres as an anode for high-rate lithium ion capacitors

Yao Jia, Zhe-wei Yang, Hui-jun Li, Yong-zhen Wang, Xiao-min Wang
1. College of Materials Science and Engineering, Taiyuan University of Technology, Taiyuan 030024, China;
2. Shanxi Key Laboratory of New Energy Materials and Devices, Taiyuan 030024, China

Corresponding authors: Xiaomin Wang, Professor, E-mail: wangxiaomin@tyut.edu.cn

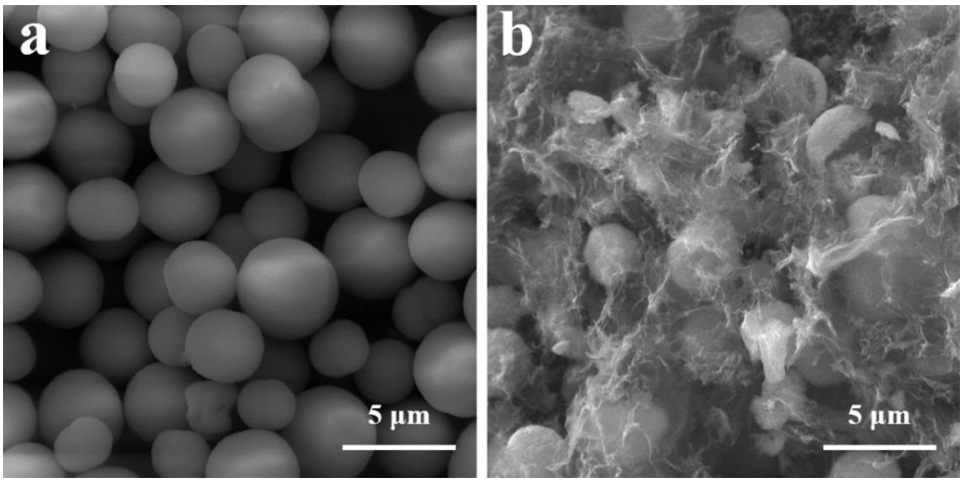

图 S1（a）$MnCO_3$和（b）$MnCO_3$/rGO 的 SEM 图

Fig. S1 SEM images of (a) $MnCO_3$ and (b) $MnCO_3$/rGO.

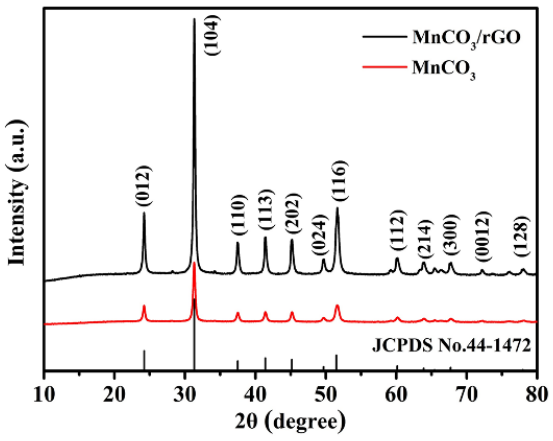

图 S2 $MnCO_3$/rGO 和 $MnCO_3$ 的 XRD 图谱

Fig. S2 XRD patterns of $MnCO_3$/rGO and $MnCO_3$.

As shown in Fig. S2, the pattern of $MnCO_3$/rGO and $MnCO_3$ displays the characteristic peaks at 24.3°, 31.4°, 37.6 °, 41.5°, 45.2°, 50.0°, 51.7°, 60.2°, 64.0°, 67.7°, 78.0° and 88.8°, corresponding to a rhodochrosite-type $MnCO_3$ crystals (JCPDS No. 44-1472) [1]. In addition, an weak peak at 20−30° can be attributed to (002) plane of rGO for MnCO3/rGO.

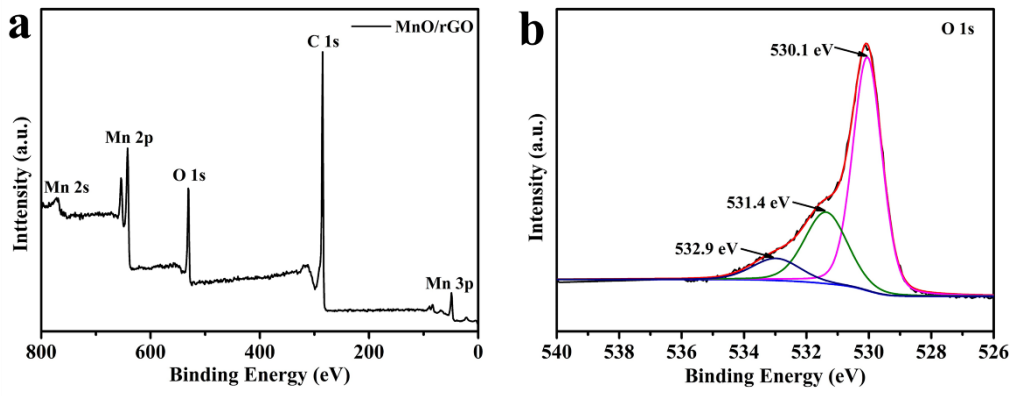

图 S3 MnO/rGO 的（a）XPS 总谱和（b）O 1s 高分辨率谱

Fig. S3 (a) XPS survey spectrum and (b) O 1s high-resolution spectra of MnO/rGO.

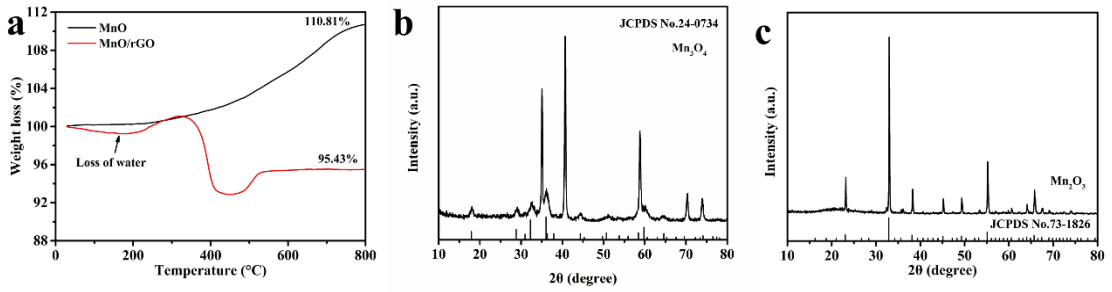

图 S4（a）MnO/rGO 和 MnO 的 TGA 曲线；空气气氛下处理 MnO/rGO 的 XRD 图（b）200℃和（c）800℃

Fig. S4 (a) TGA curves of MnO/rGO and MnO; XRD pattern of MnO/rGO treated under air atmosphere at (b) 200 ℃ and (c) 800 ℃.

As shown in Fig. S4, the drop in initial mass of MnO/rGO is due to the presence of the water in the sample. Subsequently, the mass raise is attributed to the oxidation of MnO to Mn_3O_4 (Fig. S4b) [2, 3]. Notably, the reason for the mass decrease is owing to the C in MnO/rGO was oxidized to form CO_2 with increasing temperature. Certainly, the material mass first rises and then tends to be flat because Mn_3O_4 was

further oxidized to Mn_2O_3 (Fig. S4c) when the temperature continues to rise [4].

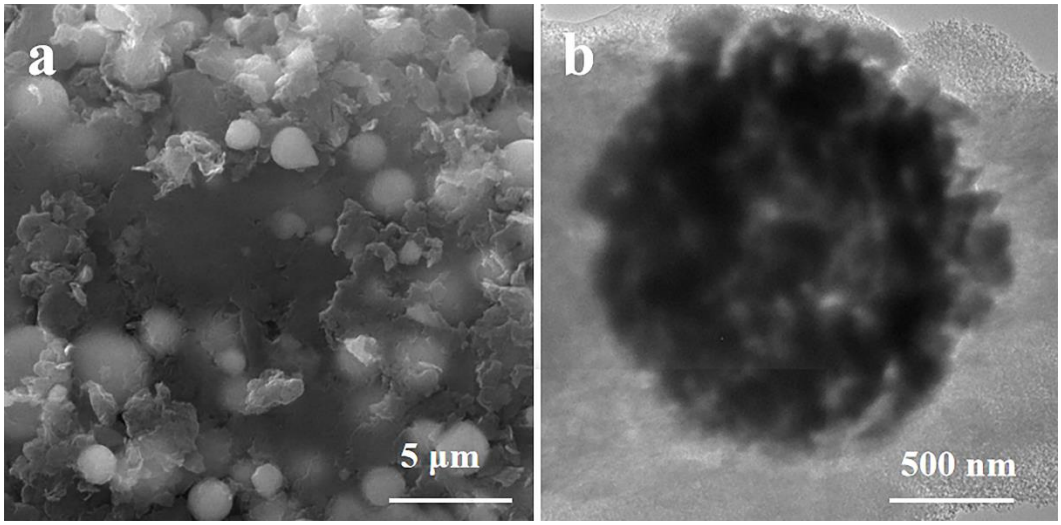

图 5 MnO/rGO 在 0.1 A g^{-1} 下循环 110 圈后的（a）SEM 图；（b）TEM 图

Fig. S5 (a) SEM image and (b) TEM image of MnO/rGO over 110 cycles at 0.1 A g^{-1}.

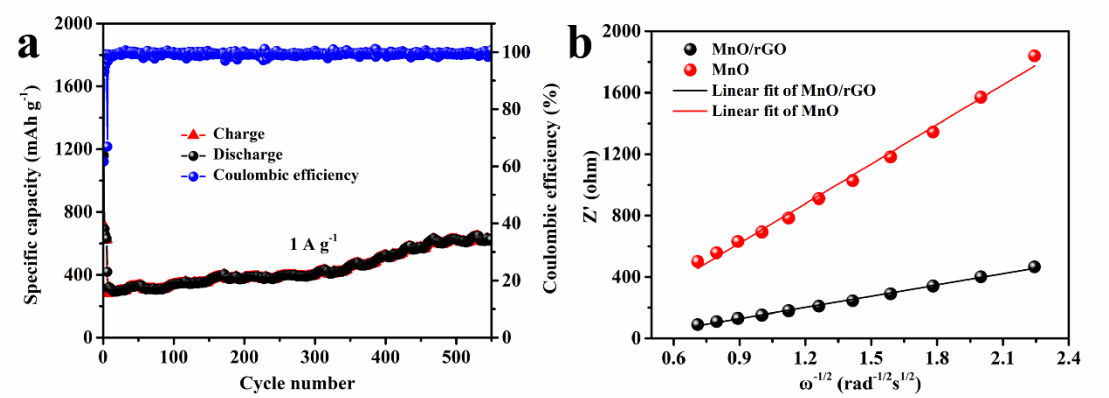

图 S6（a）MnO/rGO 在 1 A g^{-1} 下的循环性能；（b）图 4f 中 MnO/rGO 和 MnO 的低频区域的线性拟合

Fig. S6 (a) Cycling performance of MnO/rGO at 1 A g^{-1}; (b) linear fits of low-frequency region of MnO/rGO and MnO in Fig. 4f.

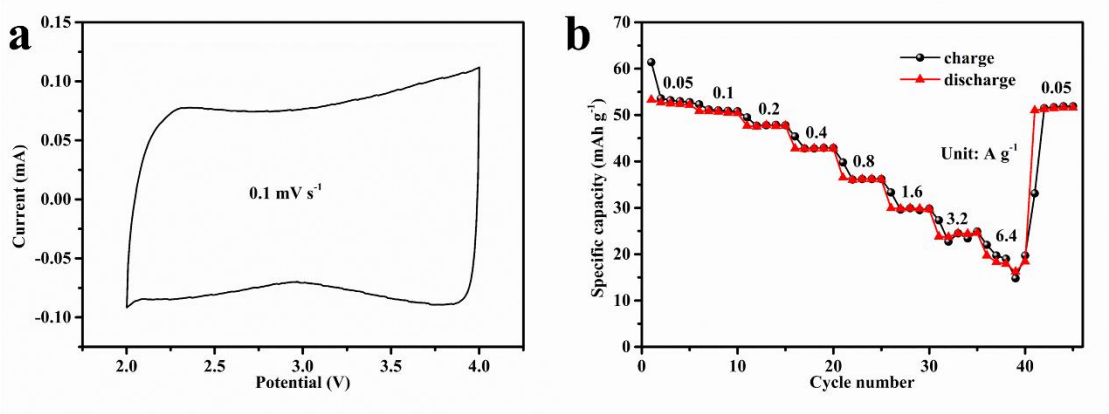

图 S7 AC 的（a）在 0.1 mV s^{-1} 扫速下 CV 曲线；（b）倍率性能

Fig. S7 (a) CV curve at 0.1 mV s^{-1} and (b) rate capability of AC

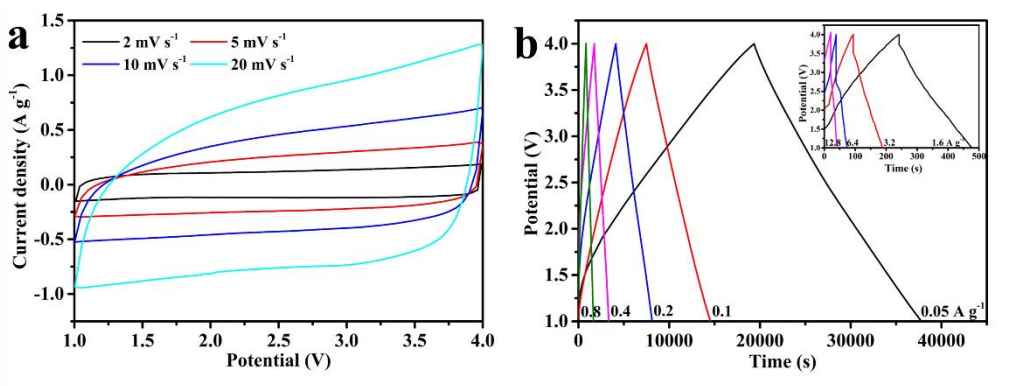

图 S8（a）在 2~20 mV s^{-1} 扫速下 LIC-3 的 CV 曲线；（b）LIC-3 在 0.05、0.1、0.2、0.4、0.8、1.6、3.2、6.4 和 12.8 A g^{-1} 电流密度下的 GCD 曲线

Fig. S8 (a) CV curves of LIC-3 at different scan rates ranging from 2 to 20 mV s^{-1}; (b) GCD curves of LIC-3 at 0.05, 0.1, 0.2, 0.4, 0.8, 1.6, 3.2, 6.4 and 12.8 A g^{-1}.

Reference

[1] Kong X, Wang Y, Lin J, Liang S, Pan A, Cao G. Twin-nanoplate assembled hierarchical Ni/MnO porous microspheres as advanced anode materials for lithium-ion batteries [J]. Electrochimica Acta, 2018, 259: 419-426.

[2] Zhang F, Wang Y, Guo W, Rao S, Mao P. Synthesis of Sn-MnO@nitrogen-doped carbon yolk-shelled three-dimensional interconnected networks as a high-performance anode material for lithium-ion batteries [J]. Chemical Engineering Journal, 2019, 360: 1509-1516.

[3] Wang J, Liu H, Liu H, Fu Z, Nan D. Facile synthesis of microsized MnO/C composites with high tap density as high performance anodes for Li-ion batteries [J]. Chemical Engineering Journal, 2017, 328: 591-598.

[4] Liu PP, Yang LY, Liu W, Zhang Y, Wang HL, Liu S, Yang RR, Guo YQ, Cui YP. TG-Novel hybrid anode of MnO nanoparticles and ultrathin carbon sheets for high lithium storage performance [J]. Journal of Alloys and Compounds, 2018, 740: 375-381.